Title

Extending optical chemical tools and technologies to mice by shifting to the shortwave infrared region

Authors

Wong, Kelly CY
Sletten, Ellen M

Publication Date

2022-06-01

DOI

10.1016/j.cbpa.2022.102131

Peer reviewed

HHS Public Access

Author manuscript

Curr Opin Chem Biol. Author manuscript; available in PMC 2023 June 01.

Published in final edited form as:

Curr Opin Chem Biol. 2022 June ; 68: 102131. doi:10.1016/j.cbpa.2022.102131.

Extending optical chemical tools and technologies to mice by shifting to the shortwave infrared region

Kelly C. Y. Wong,

Ellen M. Sletten

Department of Chemistry and Biochemistry, University of California, Los Angeles, Los Angeles, California, 90095, United States

Abstract

Fluorescence imaging is an indispensable method for studying biological processes non-invasively in cells and transparent organisms. Extension into the shortwave infrared (SWIR, 1000–2000 nm) region of the electromagnetic spectrum has allowed for imaging in mammals with unprecedented depth and resolution for optical imaging. In this review, we summarize recent advances in imaging technologies, dye scaffold modifications, and incorporation of these dyes into probes for SWIR imaging in mice. Finally, we offer an outlook on the future of SWIR detection in the field of chemical biology.

Keywords

Shortwave infrared; Fluorophore; Small molecule dye; Multiplexed imaging; Multicolor imaging; Confocal microscopy; Light-sheet microscopy; Molecular imaging; Targeted imaging; Fluorogenic probe; Ratiometric probe

Introduction

The ability to monitor dynamic processes without perturbing living systems is a hallmark of chemical biology. A common approach toward visualizing biological processes in real time is fluorescence imaging. While many fluorophores and technologies are available for imaging cells and transparent organisms [1–3], the use of optical imaging in mammals is limited by background autofluorescence and poor light penetration through tissue.

Recent developments in small animal imaging employ detection in the “biologically transparent” shortwave infrared region of the electromagnetic spectrum (SWIR or NIR-II, 1000–2000 nm). This region provides *in vivo* optical imaging with sub-millimeter resolution [4]. The benefits of the SWIR region were initially showcased with nanomaterials [5–7], which have since been optimized for use as bright biosensors [8,9] and contrast agents [10,11]. However, a recent explosion of interest in SWIR-emissive small molecule

Corresponding author: Sletten, Ellen M (sletten@chem.ucla.edu).

Declaration of competing interest

The authors declare that they have no known competing financial interests or personal relationships that could have appeared to influence the work reported in this paper.

fluorophores has paralleled SWIR nanoparticle development and facilitated the creation of minimally perturbing, non-toxic SWIR probes. These optimized SWIR fluorophores, coupled with instrumentation advancements, will render ubiquitous chemical biology techniques more effective in animals.

SWIR imaging technologies and fluorophores

Traditional fluorescence imaging utilizes the visible (VIS, 400–700 nm) and near infrared (NIR, 700–1000 nm) regions of the electromagnetic spectrum (Figure 1a). The transition from these regions to the SWIR region results in favorable imaging conditions including reduced fluorescence from endogenous chromophores, decreased light scattering by tissue [4,12,13], and increased image contrast caused by water absorption [14]. These properties result in greater imaging depths and/or resolutions compared to VIS/NIR fluorescence imaging and improve *in vivo* imaging in mammals. We highlight the main advances in technology and fluorophore development necessary to leverage the SWIR region for chemical biology.

Technologies for SWIR bioimaging

Over the past decade, many imaging technologies have been adapted for the SWIR region. The major advance in SWIR detection has been the availability of indium gallium arsenide (InGaAs) detectors which are sensitive to 950–1700 nm light [15]. Challenges of this region such as the low fluorescence quantum yield (Φ_F) of SWIR contrast agents, and the differing depths or resolutions that can be achieved depending on detection wavelengths, provide additional considerations for technology development [16,17].

Single-color SWIR imaging—Simple single-color whole mouse imaging in the SWIR was first reported in 2009 by Dai and coworkers [5]. This report showcased the advantageous properties of the SWIR region; however, imaging rates were limited by the brightness of the carbon nanotube contrast agents. The brightness of a contrast agent in an imaging experiment is quantified as the product of the absorption coefficient (ε) at the wavelength of excitation and the Φ_F at the wavelengths collected. Due to the inherently low Φ_F values in SWIR dyes [17], efficient excitation is crucial for maximized detection. Optimal single-color imaging is achieved via excitation near the wavelength of absorbance where the ε is largest ($\lambda_{max,abs}$). This fact has prompted the development of fluorophores with $\lambda_{max,abs}$ near the readily available 1064 nm laser line (see Dye scaffolds for SWIR bioimaging).

Ideally, a detection window is utilized which includes the emission peak of the fluorophore ($\lambda_{max,em}$) (Figure 1b); however, some NIR dyes with broad or tailing fluorescence profiles can be used as SWIR contrast agents by detecting the tail region of their emission spectra (Figure 1c) [18–20]. A notable example is indocyanine green (**ICG**), a clinically approved NIR fluorophore with a SWIR tail [21] which has facilitated *in vivo* SWIR imaging [18,19] and image-guided surgery [22].

Multicolor SWIR imaging—Multicolor imaging is important for studies involving ratiometric detection and (co)localization. A major asset of the SWIR window is that

it extends the range of wavelengths available for fluorescence imaging; thus, employing this region benefits studies where the detection of multiple contrast agents is necessary. Multicolor imaging often utilizes one excitation wavelength for multiple contrast agents which are detected in separate emission windows (Figure 1d). The first multicolor SWIR work detected three contrast agents in mouse brain tissues across different NIR and SWIR windows [23]. Other early works reported *in vivo* multicolor imaging of ovaries [24] and xenograft tumors [25–27] using different classes of contrast agents and/or image processing procedures.

Alternatively, multicolor imaging is achieved through orthogonal excitation of dyes with spectrally separated absorbance profiles (Figure 1e). Cosco et al. reported excitation-based multiplexed imaging where dyes are excited using distinct laser lines and emission is detected in one SWIR window, removing differences in depth/resolution between channels. This setup maximizes signal through excitation near $\lambda_{max,abs}$ and produced video-rate images in mice in three [28] and four colors [29]. Another advantage of excitation multiplexing is that crosstalk between fluorophores only occurs in one direction. In the initial report [28], this crosstalk was removed via subtraction; in the subsequent report [29], optimization of the dosing or laser power reduced the need for unmixing. Zhou and coworkers reported a similar excitation-based approach for multicolor imaging of lanthanide-doped nanoparticles [30].

2D and 3D SWIR imaging—Whole animal imaging (Figure 1f) allows for real-time micron resolution images but does not provide detailed tomographic or cellular information. For these applications, confocal and light-sheet microscopy (LSM) are necessary. Early reports of home-built SWIR confocal microscopes (Figure 1g) incorporated SWIR-compatible detectors to achieve 3D renderings of mouse brain tissue [23], ovaries [24], chloroplasts [31], tissues *ex vivo* [26], and cerebrovasculature in animals [26,32–34].

Complementary to point-by-point confocal imaging, LSM functions by illuminating samples with planar sections of light (Figure 1h). However, the use of widefield detection limits the resolution of LSM due to light scattering. Dai and coworkers overcame this limitation by constructing a SWIR LSM system [35], which was further optimized to perform structured illumination microscopy on xenograft tumors with high contrast and resolution [36].

Dye scaffolds for SWIR bioimaging

A major limitation of early SWIR imaging efforts was the dearth of small molecule fluorophores for the SWIR region. Indeed, many of the technological advances highlighted above were first demonstrated with nanomaterials. The ideal SWIR fluorophore has $\lambda_{max,em}$>1000 nm, a narrow NIR or SWIR absorption band with high ε, and a large Stokes shift with a Φ_F that is optimized for the region of the SWIR in which the fluorophore emits. It is difficult to pinpoint an exact Φ_F threshold for SWIR fluorophores due to the significant differences in Φ_F predicted by the energy gap laws [17] and the large role that solvent plays [37,38]. Note that Φ_F values are often increased in organic solvents where non-radiative pathways facilitated by H-bonding and O–H vibrational modes are minimized.

In this section, we highlight the three key scaffolds that have produced the majority of SWIR fluorophores to date.

Donor-Acceptor-Donor dyes—Donor-Acceptor-Donor (D-A-D) fluorophores are composed of two electron donating moieties flanking an electron-poor core. The first small molecule for bioimaging beyond 1000 nm was reported by Dai and coworkers who PEGylated D-A-D chromophore **M1** (**1**, Figure 2a) previously prepared for organic lightemitting diodes [39] to yield **CH1055-PEG** (**2**, Figure 2a). **CH1055-PEG** has a broad NIR absorbance and large Stokes shift (305 nm) and yielded high resolution single-color lymphatic and cerebrovascular imaging with 808 nm excitation [40]. While **CH1055-PEG** was a significant milestone for the field, major improvements to the D-A-D scaffold have occurred. Yang and coworkers replaced the classic sulfur-containing benzobisthiadiazole acceptor with its selenium congener to access longer wavelengths ($\lambda_{max,abs}$=820 nm, $\lambda_{max,em}$=1080 nm) [41]. Donor moieties can also modulate D-A-D performance through backbone distortion [41–44]. Significant improvements in Φ_F were obtained upon inclusion of shielding (S) groups to afford S-D-A-D-S fluorophores (Figure 2a) [42–44]. Although much work has been performed to optimize D-A-D dyes for SWIR bioimaging, the brightness of these fluorophores remains restricted by low ε values [19].

Polymethine dyes—Polymethine dyes consist of two heterocycles connected by a namesake methine linker. Polymethine fluorophores often have decreased Stokes shifts, photo-stability, and Φ_F values compared to D-A-D dyes. However, their high ε, narrow absorption bands, scaffold tunability, and extended emission tails have made them excellent SWIR emitters [45].

The exceptional absorption properties of polymethine dyes are evident in the success of **ICG** (**3**, Figure 2b) as a SWIR contrast agent even when only 5% of its emission is collected [19,21]. Strategies to red-shift **3** into the SWIR through both heterocycle [46–48] and polymethine chain modification [49,50] have been performed. Notable heterocycle advances include: 1) the benzo[c,d]indolium heterocycle, first reported by Henary et al. [46] and named/applied to *in vivo* imaging by Zhang and coworkers (**4**, **FD-1080**, Figure 2b) [47]; 2) appending extra indolium heterocycles to produce tetra-indolium dye **LZ-1105** [48]. Polymethine dye extension has resulted in variants of **3** (**ICG-C11**) [49] and aryl-fused nonamethine dyes (**FNIR-1072**, **5**, Figure 2b) [50]. Fluorophores **4**, **5**, and **LZ-1105** can all be imaged with excitation at 1064 nm. Schnermann and coworkers demonstrated three-color excitation-multiplexed imaging using **3**, **5**, and nonamethine **FNIR-872** [50].

The use of heteroatoms other than nitrogen in polymethine dye heterocycles has also been fruitful towards the creation of SWIR fluorophores. This work builds off thiaflavylium dye **IR-26** (**6**, Figure 2b) and thiapyrylium dye **IR-1061**. Optimization of sulfur-containing dyes has yielded pentamethine dyes **BTC1070** [51] and **5H5** [52]. While sulfur provides impressive red-shifts, non-radiative pathways may be facilitated by heavy atoms. Consequently, oxygen-containing heterocycles have been explored. The first polymethine designed for SWIR imaging, **Flav7** (**7**, Figure 2b), was inspired by **6** with replacement of sulfur with oxygen and the addition of an electron donating dimethylamino group. **Flav7** exhibited a Φ_F ten-fold greater than **6** while maintaining $\lambda_{max,abs}$>1000 nm [53].

Further optimization has yielded fluorophores that can be excited at 1064 nm (**JuloFlav7**, $\lambda_{max,abs}$=1061 nm) [28] and fluorophores with increased brightness (**Chrom7**, Φ_F=1.7%) [29] (Figure 2b). Zhang and coworkers have also developed a series of chromenylium dyes coined **CX** dyes with impressive chemo- and photostability [54].

BODIPY and aza-BODIPY dyes—Boron-dipyrromethene (BODIPY) difluoride dyes and their derivatives have recently gained interest as SWIR emitters. BODIPYs display excellent Φ_F values and stability and can be red-shifted through nitrogen incorporation [55]. First synthesized in 2002 as promising phototherapeutic agents [56] (**8**, Figure 2c), aza-BODIPYs have high ε, large Stokes shifts, and $\lambda_{max,abs}$ values spanning the NIR region [55–57]. Two teams concurrently reported the first SWIR aza-BODIPY contrast agents in 2019. Huang and coworkers appended electron donating moieties to the aza-BODIPY core to produce D-A-D-like dyes **NJ1030** and **NJ1060** ($\lambda_{max,em}$=1030 and 1060 nm) [58]. In contrast, Sancey et al. synthesized blue-shifted **aza-SWIR-01** ($\lambda_{max,em}$=980 nm, **9**, Figure 2c). Ammonium groups were appended to **10** to produce water-soluble **SWIR-WAZABY-01** (**10**, Figure 2c), which was employed for single-color emission tail imaging in mice [59].

Small molecule SWIR probes

A prominent avenue of chemical biology is modifying fluorophores such that they provide a functional readout on a biological system as fluorescent “probes”. Initial reports toward SWIR probes are highlighted below.

Targeted and molecular imaging probes

Targeted probes consist of fluorophores conjugated to agents which label specific biomolecules, metabolites, or tissues. The first reported small molecule SWIR molecular imaging probe consisted of D-A-D dye **CH1055** conjugated to an anti-EGFR affibody [40]. S-D-A-D-S probes have also been conjugated to chorionic gonadotropin and poly-L-lysine for hormone receptor imaging [24] and dendritic cell tracking (Table 1, entry 1) [60], respectively. Additionally, Tan and coworkers used a tetraazido D-A-D dye [23] to label *D*-propargyl glycine in gut microbiota via *ex vivo* click chemistry (**11**, Figure 3a; Table 1, entry 2). The labeled microbes were administered back to mice via gavage and imaged [61].

Polymethine dye conjugates have also been utilized as targeted imaging agents, with most relying on antibodies or cyclic RGD peptide (cRGD) for targeting. A **IRDye 800CW**-trastuzumab conjugate was used by Carr et al. for SWIR tail imaging of xenografts in 2018 [19]. Both **ICG-C11** and the nonamethine **FNIR-872** have been conjugated to antibodies for labeling overexpressed receptors in xenograft tumors (Table 1, entries 4, 5) [49,50]. The xenograft imaging with **FNIR-872** was paired with a nonamethine-dextran conjugate (Table 1, entry 5) and **3** to simultaneously observe the surrounding lymphatics and vasculature [50]. $\alpha_v\beta_3$ integrin targeting has also been a popular approach for targeted imaging with polymethine dyes including thiapyrylium (Table 1, entry 6) [52], benzo[c,d]indolium (Table 1, entry 7) [62], and thiaflavylium (Table 1, entry 8) [63] dye-cRGD conjugates.

Fluorogenic and ratiometric probes

Compared to “always-on” dye conjugates for molecular imaging, responsive fluorescent probes display higher specificity. Fluorogenic or “turn-on” probes display enhanced Φ_F in response to a stimulus, while ratiometric probes can monitor subtle changes to stimuli by using ratios between multiple signals. In the past three years, SWIR dyes have been developed into a number of stimuli-responsive probes for *in vivo* detection.

Metabolite detection in the SWIR region has enabled diagnostics in animal disease models. Early reports of metabolite-responsive SWIR probes include BODIPY-based fluorogenic probes for H_2S detection [64] and a hydroxyl radical-reactive fluorogenic cyanine probe [65]. A recent development in ratiometric SWIR probes is a micellar hydrogen peroxide-activated probe by Yang et al. (Table 1, entry 3) which involves chemiluminescence energy transfer from H_2O_2-generated dioxetanedione to a D-A-D dye, followed by Förster resonance energy transfer (FRET) to a second D-A-D fluorophore [66]. Multiple SWIR probes have also been developed for peroxynitrite ($ONOO^-$) detection. Lei et al. found that polymethine dyes **CX-1** and **CX-3** formed a highly efficient FRET pair when encapsulated in micelles, with the latter being susceptible to oxidative degradation by $ONOO^-$ (Table 1, entry 11) [54]. Li et al. developed polymethine probe **IRBTP-B** (**12**, Figure 3b; Table 1, entry 9) by including a phenyl boronate ester which yields a non-emissive species until uncaged by $ONOO^-$ [67]. Finally, a carboxylated **LZ-1105** derivative (Table 1, entry 12) was paired with lanthanide-doped nanoparticles to detect $ONOO^-$ levels [68].

Two pH-sensitive thiapyrylium probes were recently designed by Zhang and coworkers. One probe exhibited ratiometric fluctuations in emission intensity based on protonation states of the dimethylamino substituents (Table 1, entry 13) [51]. Another employed PEGylated dye aggregate **CEAF-OMe** (**13**, Figure 3c; Table 1, entry 10), which exhibited aggregation-induced quenching when neutrally charged and displayed a 72-fold signal increase upon endocytosis [63].

Dye precursor-enzyme substrate conjugates have been reported as enzyme-responsive SWIR probes. Wang et al. created three indolium-substituted BODIPY probes (Table 1, entry 14) which were conjugated to substrates for nitroreductase (NTR), NAD(P)H quinone oxidoreductase isozyme 1 (NQO), or alkaline phosphatase (ALP) via a benzothioether linker. In a mechanism analogous to **12**, substrate cleavage and linker elimination resulted in a dye with SWIR tail emission (**14**, Figure 3d) [69]. A similar β-galactosidase-responsive probe was also developed (Table 1, entry 15) [70].

Unlike aforementioned probes, fluorescence of BODIPY probe **WD-NO_2** (**15**, Figure 3e; Table 1, entry 16) is activated by a physical stimulus. This probe by Liu and coworkers possesses a rotating piperidinyl “spin group” which rigidifies in viscous environments such as inflamed tissues (Figure 3e). Rigidification favors fluorophore backbone conjugation to yield a ~5-fold increase in brightness *in vivo* [71].

Conclusions and outlook

Expansion of optical imaging into the SWIR window has revolutionized non-invasive imaging and detection within mammals. Much work has been done to adapt pre-existing technologies for SWIR imaging. Concurrently, the development of bright, robust fluorophores is necessary for chemical biology studies *in vivo*. As highlighted here, significant work has been performed to create such contrast agents for the SWIR window. The tuning of D-A-D, polymethine, and aza-BODIPY scaffolds has resulted in SWIR dyes with enhanced brightness and utility in living systems. Recent work transforming these SWIR dyes into fluorogenic and ratiometric probes demonstrates great potential for the creation of chemical tools that can be visualized non-invasively in mice. This work aims to bridge the gap between fundamental studies in cells and translational research in mammals.

Still, there is ample space for the development of SWIR technologies and probes. Techniques such as multi-photon excitation [72] are now being adapted for the SWIR region. Opportunities remain for expansion and/or optimization of such advanced optical imaging technologies for this window. Further development and availability of SWIR-compatible microscopes, flow cytometers, and plate readers is also essential to fully integrate the SWIR region into standard chemical biology procedures. Other fluorophore scaffolds such as xanthene [73] and squaraine [74,75] are showing potential as SWIR contrast agents. We anticipate further advancements in SWIR probes including ion sensing, fluorogens, and turn-on FRET probes, which will be powerful additions to the optical imaging toolbox for non-invasive detection in mammals.

Acknowledgements

The authors thank Dr. Shang Jia, Irene Lim, Anthony Spearman, Cesar Garcia, and Emily Mobley for critical reading of this review.

Funding sources

This work was supported by a fellowship to K. C. Y. Wong from the National Science Foundation (DGE-2034835). We thank the following funding sources for supporting the red-shifted chromophore work within our group: NIBIB (5R01EB027172), NIGMS (5R01GM135380), NSF (CHE-1905242), and Alfred P. Sloan Foundation (FG-2018-10855).

Abbreviations

SWIR	shortwave infrared
VIS	visible
NIR	near infrared
ICG	indocyanine green
InGaAs	indium gallium arsenide
LSM	light-sheet microscopy
D-A-D	donor-acceptor-donor

PEG	polyethylene glycol
EGFR	epidermal growth factor receptor
FRET	Förster resonance energy transfer
NTR	nitroreductase
NQO	NAD(P)H:quinone oxidoreductase isozyme 1
ALP	alkaline phosphatase
Mon	monensin
Nys	nystatin
LPS	lipopolysaccharide
FBS	fetal bovine serum
PBS	phosphate buffered saline
DMSO	dimethyl sulfoxide

References

Papers of particular interest, published within the period of review, have been highlighted as:

* of special interest

1. Johnsson N, Johnsson K: Chemical tools for biomolecular imaging. ACS Chem Biol 2007, 2:31–38, 10.1021/cb6003977. [PubMed: 17243781]
2. Lavis LD, Raines RT: Bright ideas for chemical biology. ACS Chem Biol 2008, 3:142–155, 10.1021/cb700248m. [PubMed: 18355003]
3. Grimm JB, Lavis LD: Caveat fluorophore: an insiders' guide to small-molecule fluorescent labels. Nat Methods 2021, 10.1038/s41592-021-01338-6.
4. Hong G, Antaris AL, Dai H: Near-infrared fluorophores for biomedical imaging. Nat Biomed Eng 2017, 1, 0010, 10.1038/s41551-016-0010.
5. Welsher K, Liu Z, Sherlock SP, Robinson JT, Chen Z, Daranciang D, Dai H: A route to brightly fluorescent carbon nanotubes for near-infrared imaging in mice. Nat Nanotechnol 2009, 4:773–780, 10.1038/nnano.2009.294. [PubMed: 19893526]
6. Naczynski DJ, Tan MC, Zevon M, Wall B, Kohl J, Kulesa A, Chen S, Roth CM, Riman RE, Moghe PV: Rare-earth-doped biological composites as in vivo shortwave infrared reporters. Nat Commun 2013, 4:2199, 10.1038/ncomms3199. [PubMed: 23873342]
7. Hong G, Robinson JT, Zhang Y, Diao S, Antaris AL, Wang Q, Dai H: In vivo fluorescence imaging with Ag_2S quantum dots in the second near-infrared region. Angew Chem Int Ed 2012, 51:9818–9821, 10.1002/anie.201206059.
8. Jain A, Homayoun A, Bannister CW, Yum K: Single-walled carbon nanotubes as near-infrared optical biosensors for life sciences and biomedicine. Biotechnol J 2015, 10:447–459, 10.1002/biot.201400168. [PubMed: 25676253]
9. Gong L, Shan X, Zhao XH, Tang L, Zhang XB: Activatable NIR-II fluorescent probes applied in biomedicine: progress and perspectives. ChemMedChem 2021, 16:1–16, 10.1002/cmdc.202100142.
10. Zhong Y, Ma Z, Wang F, Wang X, Yang Y, Liu Y, Zhao X, Li J, Du H, Zhang M, Cui Q, Zhu S, Sun Q, Wan H, Tian Y, Liu Q, Wang W, Garcia KC, Dai H: In vivo molecular imaging for

immunotherapy using ultra-bright near-infrared-IIb rare-earth nanoparticles. Nat Biotechnol 2019, 37:1322–1331, 10.1038/s41587-019-0262-4. [PubMed: 31570897]

11. Cao J, Zhu B, Zheng K, He S, Meng L, Song J, Yang H: Recent progress in NIR-II contrast agent for biological imaging. Front Bioeng Biotechnol 2020, 7:487, 10.3389/fbioe.2019.00487. [PubMed: 32083067]
12. Lim YT, Kim S, Nakayama A, Stott NE, Bawendi MG, Frangioni JV: Selection of quantum dot wavelengths for biomedical assays and imaging. Mol Imag 2003, 2:50–64, 10.1162/15353500200302163.
13. Zhang H, Salo DC, Kim DM, Komarov S, Tai Y-C, Berezin MY: Penetration depth of photons in biological tissues from hyperspectral imaging in shortwave infrared in transmission and reflection geometries. J Biomed Opt 2016, 21:126006, 10.1117/1.JBO.21.12.126006.
14. Carr JA, Aellen M, Franke D, So PTC, Bruns OT, Bawendi MG: Absorption by water increases fluorescence image contrast of biological tissue in the shortwave infrared. Proc Natl Acad Sci USA 2018, 115:9080–9085, 10.1073/pnas.1803210115. [PubMed: 30150372]
15. Smith M, Mancini MC, Nie S: Second window for in vivo imaging. Nat Nanotechnol 2009, 4:710–711, 10.1038/nnano.2009.326. [PubMed: 19898521]
16. Thimsen E, Sadtler B, Berezin MY: Shortwave-infrared (SWIR) emitters for biological imaging: a review of challenges and opportunities. Nanophotonics 2017, 6:1043–1054, 10.1515/nanoph-2017-0039.
17*. Friedman HC, Cosco ED, Atallah TL, Jia S, Sletten EM, Caram JR: Establishing design principles for emissive organic SWIR chromophores from energy gap laws. Chem 2021, 7:3359–3376, 10.1016/j.chempr.2021.09.001. [PubMed: 34901520] The authors establish an equation which predicts the fluorescence quantum yield limits for SWIR fluorophores. The insight gained from this work can be applied to design SWIR dyes with improved brightness.
18. Starosolski Z, Bhavane R, Ghaghada KB, Vasudevan SA, Kaay A, Annapragada A: Indocyanine green fluorescence in second near-infrared (NIR-II) window. PLoS One 2017, 12, e0187563, 10.1371/journal.pone.0187563.
19. Carr JA, Franke D, Caram JR, Perkinson CF, Saif M, Askoxylakis V, Datta M, Fukumura D, Jain RK, Bawendi MG, Bruns OT: Shortwave infrared fluorescence imaging with the clinically approved near-infrared dye indocyanine green. Proc Natl Acad Sci USA 2018, 115:4465–4470, 10.1073/pnas.1718917115. [PubMed: 29626132]
20. Zhu S, Yung BC, Chandra S, Niu G, Antaris AL, Chen X: Near-Infrared-II (NIR-II) bioimaging via off-peak NIR-I fluorescence emission. Theranostics 2018, 8:4141–4151, 10.7150/thno.27995. [PubMed: 30128042]
21. Cosco ED, Lim I, Sletten EM: Photophysical properties of indocyanine green in the shortwave infrared region. Chem-PhotoChem 2021, 5:727–734, 10.1002/cptc.202100045.
22*. Hu Z, Fang C, Li B, Zhang Z, Cao C, Cai M, Su S, Sun X, Shi X, Li C, Zhou T, Zhang Y, Chi C, He P, Xia X, Chen Y, Gambhir SS, Cheng Z, Tian J: First-in-human liver-tumour surgery guided by multispectral fluorescence imaging in the visible and near-infrared-I/II windows. Nat Biomed Eng 2019, 4:259–271, 10.1038/s41551-019-0494-0. [PubMed: 31873212] Liver tumor resection is performed using a multispectral instrument spanning the visible, NIR, and SWIR regions with ICG as a contrast agent. This represents the first report of SWIR imaging for fluorescence-guided surgery in humans.
23. Zhu S, Yang Q, Antaris AL, Yue J, Ma Z, Wang H, Huang W, Wan H, Wang J, Diao S, Zhang B, Li X, Zhong Y, Yu K, Hong G, Luo J, Liang Y, Dai H: Molecular imaging of biological systems with a clickable dye in the broad 800- to 1,700-nm near-infrared window. Proc Natl Acad Sci USA 2017, 114:962–967, 10.1073/pnas.1617990114. [PubMed: 28096386]
24. Zhu S, Herraiz S, Yue J, Zhang M, Wan H, Yang Q, Ma Z, Wang Y, He J, Antaris AL, Zhong Y, Diao S, Feng Y, Zhou Y, Yu K, Hong G, Liang Y, Hsueh AJ, Dai H: 3D NIR-II molecular imaging distinguishes targeted organs with high-performance NIR-II bioconjugates. Adv Mater 2018, 30:1705799, 10.1002/adma.201705799.
25. Bruns OT, Bischof TS, Harris DK, Franke D, Shi Y, Riedemann L, Bartelt A, Jaworski FB, Carr JA, Rowlands CJ, Wilson MWB, Chen O, Wei H, Hwang GW, Montana DM, Coropceanu I, Achorn OB, Kloepper J, Heeren J, So PTC, Fukumura D, Jensen JF, Jain RJ, Bawendi MG:

Next-generation in vivo optical imaging with short-wave infrared quantum dots. Nat Biomed Eng 2017, 1, 0056, 10.1038/s41551-017-0056.

26. Wan H, Yue J, Zhu S, Uno T, Zhang X, Yang Q, Yu K, Hong G, Wang J, Li L, Ma Z, Gao H, Zhong Y, Su J, Antaris AL, Xia Y, Luo J, Liang Y, Dai H: A bright organic NIR-II nanofluorophore for three-dimensional imaging into biological tissues. Nat Commun 2018, 9:1171, 10.1038/s41467-018-03505-4. [PubMed: 29563581]
27. Tian R, Ma H, Zhu S, Lau J, Ma R, Liu Y, Lin L, Chandra S, Wang S, Zhu X, Deng JH, Niu G, Zhang M, Antaris AL, Hettie JS, Yang B, Liang Y, Chen X: Multiplexed NIR-II probes for lymph node-invaded cancer detection and imaging-guided surgery. Adv Mater 2020, 32:1907365, 10.1002/adma.201907365.
28*. Cosco ED, Spearman AL, Ramakrishnan S, Lingg JGP, Saccomano M, Pengshung M, Arús BA, Wong KCY, Glasl S, Ntziachristos V, Warmer M, McLaughlin RR, Bruns OT, Sletten EM: Shortwave infrared polymethine fluorophores matched to excitation lasers enable non-invasive, multi-colour *in vivo* imaging in real time. Nat Chem 2020, 12: 1123–1130, 10.1038/s41557-020-00554-5. [PubMed: 33077925] Flavylium polymethine dyes matched to excitation laser lines 980 nm and 1064 nm, along with ICG, were utilized for three-color imaging in awake mice with single-channel detection. This report is the first to use excitation-multiplexed imaging in the SWIR region.
29. Cosco ED, Arús BA, Spearman AL, Atallah TL, Lim I, Leland OS, Caram JR, Bischof TS, Bruns OT, Sletten EM: Bright chromenylium polymethine dyes enable fast, four-color *in vivo* imaging with shortwave infrared detection. J Am Chem Soc 2021, 143:6836–6846, 10.1021/jacs.0c11599. [PubMed: 33939921]
30. Jia Q, Ma L, Zhai X, Fu W, Liu Y, Liao X, Zhou J: Orthogonal near-infrared-II imaging enables spatially distinguishing tissues based on lanthanide-doped nanoprobes. Anal Chem 2020, 92:14762–14768, 10.1021/acs.analchem.0c03383. [PubMed: 33085472]
31. Zubkovs V, Antonucci A, Schuergers N, Lambert B, Latini A, Ceccareli R, Santinelli A, Rogov A, Ciepielewski D, Boghossian AA: Spinning-disc confocal microscopy in the second near-infrared window (NIR-II). Sci Rep 2018, 8:13770, 10.1038/s41598-018-31928-y.
32. Yu X, Feng Z, Cai Z, Jiang M, Xue D, Zhu L, Zhang Y, Liu J, Que B, Yang W, Xi W, Zhang D, Qian J, Li G: Deciphering of cerebrovasculatures via ICG-assisted NIR-II fluorescence microscopy. J Mater Chem B 2019, 7:6623–6629, 10.1039/c9tb01381d. [PubMed: 31591622]
33. Yu W, Guo B, Zhang H, Zhou J, Yu X, Zhu L, Xue D, Liu W, Sun X, Qian J: NIR-II fluorescence in vivo confocal microscopy with aggregation-induced emission dots. Sci Bull 2019, 64:410–416, 10.1016/j.scib.2019.02.019.
34. Cai Z, Zhu L, Wang M, Roe AW, Xi W, Qian J: NIR-II fluorescence microscopic imaging of cortical vasculature in non-human primates. Theranostics 2020, 10:4265–4276, 10.7150/thno.43533. [PubMed: 32226552]
35. Wang F, Wan H, Ma Z, Zhong Y, Sun Q, Tian Y, Qu L, Du H, Zhang M, Li L, Ma H, Luo J, Liang Y, Li WJ, Hong G, Liu L, Dai H: Light-sheet microscopy in the near-infrared II window. Nat Methods 2019, 16:545–552, 10.1038/s41592-019-0398-7. [PubMed: 31086342]
36*. Wang F, Ma Z, Zhong Y, Salazar F, Xu C, Ren F, Qu L, Wu AM, Dai H: In vivo NIR-II structured-illumination light-sheet microscopy. Proc Natl Acad Sci USA 2021, 118, e2023888118, 10.1073/pnas.2023888118.A home-built light-sheet microscopy setup with structured-illumination capabilities was employed for two-color xenograft tumor imaging. This improved configuration reduced light scattering and generated images with approximately two-fold greater spatial resolution compared to a previously reported SWIR light-sheet setup.
37. Maillard J, Klehs K, Rumble C, Vauthey E, Heilemann M, Fürstenberg A: Universal quenching of common fluorescent probes by water and alcohols. Chem Sci 2021, 12:1352–1362, 10.1039/d0sc05431c.
38. Matikonda SS, Hammersley G, Kumari N, Grabenhorst L, Glembockyte V, Tinnefeld P, Ivanic J, Levitus M, Schnermann MJ: Impact of cyanine conformational restraint in the near-infrared range. J Org Chem 2020, 85:5907–5915, 10.1021/acs.joc.0c00236. [PubMed: 32275153]
39. Qian G, Dai B, Luo M, Yu D, Zhan J, Zhang Z, Ma D, Wang ZY: Band gap tunable, donor-acceptor-donor charge-transfer heteroquinoid-based chromophores: near infrared photo-luminescence and electroluminescence. Chem Mater 2008, 20:6208–6216, 10.1021/cm801911n.

40. Antaris AL, Chen H, Cheng K, Sun Y, Hong G, Qu C, Diao S, Deng Z, Hu X, Zhang B, Zhang X, Yaghi OK, Alamparambil ZR, Hong X, Chen Z, Dai H: A small-molecule dye for NIR-II imaging. Nat Mater 2016, 15:235–242, 10.1038/nmat4476. [PubMed: 26595119]

41. Zhang R, Wang Z, Xu L, Xy Y, Lin Y, Zhang Y, Sun Y, Yang G: Rational design of a multifunctional molecular dye with single dose and laser for efficiency NIR-II fluorescence/photoacoustic imaging guided photothermal therapy. Anal Chem 2019, 91:12476–12483, 10.1021/acs.analchem.9b03152. [PubMed: 31475521]

42. Yang Q, Ma Z, Wang H, Zhou B, Zhu S, Zhong Y, Wang J, Wan H, Antaris A, Ma R, Zhang X, Yang J, Zhang X, Sun H, Liu W, Liang Y, Dai H: Rational design of molecular fluorophores for biological imaging in the NIR-II window. Adv Mater 2017, 29:1605497, 10.1002/adma.201605497.

43. Ma H, Liu C, Hu Z, Yu P, Zhu X, Ma R, Sun Z, Zhang C-H, Sun H, Zhu S, Liang Y: Propylenedioxy thiophene donor to achieve NIR-II molecular fluorophores with enhanced brightness. Chem Mater 2020, 32:2061–2069, 10.1021/acs.chemmater.9b05159.

44. Yang Q, Hu Z, Zhu S, Ma R, Ma H, Ma Z, Wan H, Zhu T, Jiang Z, Liu W, Jiao L, Sun H, Liang Y, Dai H: Donor engineering for NIR-II molecular fluorophores with enhanced fluorescent performance. J Am Chem Soc 2018, 140:1715–1724, 10.1021/jacs.7b10334. [PubMed: 29337545]

45. Bricks JL, Kachkovskii AD, Slominskii YL, Gerasov AO, Popov SV: Molecular design of near infrared polymethine dyes: a review. Dyes Pigments 2015, 121:238–255, 10.1016/j.dyepig.2015.05.016.

46. Henary M, Mojzych M, Say M, Strekowski L: Functionalization of benzo[c,d]indole system for the synthesis of visible and near-infrared dyes. J Heterocycl Chem 2009, 46:84–87, 10.1002/jhet.

47. Li B, Lu L, Zhao M, Lei Z, Zhang F: An efficient 1064 nm NIR-II excitation fluorescent molecular dye for deep-tissue high-resolution dynamic bioimaging. Angew Chem Int Ed 2018, 57: 7483–7487, 10.1002/anie.201801226.

48*. Li B, Zhao M, Feng L, Dou C, Ding S, Zhou G, Lu L, Zhang H, Chen F, Li X, Li G, Zhao S, Jiang C, Wang Y, Zhao D, Chen Y, Zhang F: Organic NIR-II molecule with long blood half-life for in vivo dynamic vascular imaging. Nat Commun 2020, 11: 3102, 10.1038/s41467-020-16924-z. [PubMed: 32555157] The authors report LZ-1105, a tetra-indolium dye with a ~3.2 h blood circulation half-life. This dye facilitated mouse imaging with higher contrast, signal-to-noise ratio, and blood retention compared to imaging with ICG.

49. Swamy MMM, Murai Y, Monde K, Tsuboi S, Jin T: Shortwave-infrared fluorescent molecular imaging probes based on π-conjugation extended indocyanine green. Bioconjugate Chem 2021, 32:1541–1547, 10.1021/acs.bioconjchem.1c00253.

50*. Bandi VG, Luciano MP, Saccomano M, Patel NL, Bischof TS, Lingg JGP, Tsrunchev PT, Nix MN, Ruehle B, Sanders C, Riffle L, Robinson CM, Difilippantonio S, Kalen JD, Resch-Genger U, Ivanic J, Bruns OT, Schnermann MJ: Targeted multicolor in vivo imaging over 1000 nm enabled by nonamethine cyanines. Nature Methods 2022, 19:353–358, 10.1038/s41592-022-01394-6. [PubMed: 35228725] Antibody and dextran conjugates of nonamethine dyes FNIR-872 and FNIR-1072 were paired with heptamethine dyes with SWIR tail emission for multicolor imaging in xenograft mouse models. In addition to showcasing targeted and multiplexed imaging in the SWIR window, this work highlights methine chain modification as a method for modulating SWIR polymethine dyes.

51. Wang S, Fan Y, Li D, Sun C, Lei Z, Lu L, Wang T, Zhang F: Anti-quenching NIR-II molecular fluorophores for in vivo high-contrast imaging and pH sensing. Nat Commun 2019, 10:1058, 10.1038/s41467-019-09043-x. [PubMed: 30837470]

52. Ding B, Xiao Y, Zhou H, Zhang X, Qu C, Xu F, Deng Z, Cheng Z, Hong X: Polymethine thiopyrylium fluorophores with absorption beyond 1000 nm for biological imaging in the second near-infrared subwindow. J Med Chem 2019, 62: 2049–2059, 10.1021/acs.jmedchem.8b01682. [PubMed: 30501190]

53. Cosco ED, Caram JR, Bruns OT, Franke D, Day RA, Farr EP, Bawendi MG, Sletten EM: Flavylium polymethine fluorophores for near- and shortwave infrared imaging. Angew Chem Int Ed 2017, 56:13126–13129, 10.1002/anie.201706974.

54. Lei Z, Sun C, Pei P, Wang S, Li D, Zhang X, Zhang F: Stable, wavelength-tunable fluorescent dyes in the NIR-II region for in vivo high-contrast bioimaging and multiplexed biosensing. Angew Chem Int Ed 2019, 131:8250–8255, 10.1002/anie.201904182.

55. Shi Z, Han X, Hu W, Bai H, Peng B, Ji L, Fan Q, Li L, Huang W: Bioapplications of small molecule Aza-BODIPY: from rational structural design to in vivo investigations. Chem Soc Rev 2020, 49:7533–7567, 10.1039/D0CS00234H. [PubMed: 32996497]

56. Killoran J, Allen L, Gallagher JF, Gallagher WM, O'Shea DF: Synthesis of BF_2 chelates of tetraarylazadipyrromethenes and evidence for their photodynamic therapeutic behaviour. Chem Commun 2002:1862–1863, 10.1039/B204317C.

57. Karlsson JKG, Harriman A: Origin of the red-shifted optical spectra recorded for aza-BODIPY dyes. J Phys Chem A 2016, 120:2537–2546, 10.1021/acs.jpca.6b01278. [PubMed: 27046505]

58. Bai L, Sun P, Liu Y, Zhang H, Hu W, Zhang W, Liu Z, Fan Q, Li L, Huang W: Novel aza-BODIPY based small molecular NIR-II fluorophores for *in vivo* imaging. Chem Commun 2019, 55: 10920–10923, 10.1039/c9cc03378e.

59*. Godard A, Kalot G, Pliquett J, Busser B, Le Guevel X, Wegner KD, Resch-Genger U, Rousselin Y, Coll J-L, Denat F, Bodio E, Goze C, Sancey L: Water-soluble aza-BODIPYs: biocompatible organic dyes for high contrast *in vivo* NIR-II imaging. Bioconjugate Chem 2020, 31:1088–1092, 10.1021/acs.bioconjchem.0c00175.The authors appended ammonium groups to their previously reported SWIR-emissive fluorophore to yield aza-SWIR-01, the first water-soluble aza-BODIPY dye for detection in the SWIR window.

60. Wang C, Sun B, Bao H, Wang T, Xu W, Sun P, Fan Q, Huang W: NIR-II probe modified by poly(L-lysine) with efficient oval-bumin delivery for dendritic cell tracking. Sci China Chem 2020, 63:1272–1280, 10.1007/s11426-020-9780-8.

61*. Wang W, Yang Q, Du Y, Zhou X, Du X, Wu Q, Lin L, Song Y, Li F, Yang C: Metabolic labeling of peptidoglycan with NIR-II dye enables in vivo imaging of gut microbiota. Angew Chem Int Ed 2019, 59:2628–2633, 10.1002/anie.201910555.Gut microbiota with metabolically incorporated *D*-propargyl glycine were modified with a SWIR D-A-D dye. Microbes were imaged in live mice with time-dependent SWIR imaging. This report showcases the convergence of SWIR imaging and chemical biology.

62*. Zhao M, Ding J, Mao Q, Zhang Y, Gao Y, Ye S, Qin H, Shi H: A novel $\alpha_v\beta_3$ integrin-targeted NIR-II nanoprobe for multi-modal imaging-guided photothermal therapy of tumors *in vivo*. Nanoscale 2020, 12:6953–6958, 10.1039/c9nr10720g. [PubMed: 32191787]

63*. He Y, Wang S, Yu P, Yan K, Ming J, Yao C, He Z, El-Toni AM, Khan A, Zhu X, Sun C, Lei Z, Zhang F: NIR-II cell endocytosis-activated fluorescent probes for *in vivo* high-contrast bioimaging diagnostics. Chem Sci 2021, 12:10474–10482, 10.1039/D1SC02763H. [PubMed: 34447540] Thiaflavylium dye Lyso1005 was PEGylated and transformed into pH-sensitive probe CEAF-OMe, which exhibited fluorescence turn-on behavior when protonated. CEAF-OMe and cRGD-targeted probe CEAF-RGD were used to image xenograft tumors and an arthritic mouse model, respectively.

64. Xu G, Yan Q, Lv X, Zhu Y, Xin K, Shi B, Wang R, Chen J, Gao W, Shi P, Fan C, Zhao C, Tian H: Imaging of colorectal cancers using activatable nanoprobes with second near-infrared window emission. Angew Chem Int Ed 2018, 57:3626–3630, 10.1002/anie.201712528.

65. Feng W, Zhang Y, Li Z, Zhai S, Lv W, Liu Z: Lighting up NIR-II fluorescence in vivo: an activable probe for non-invasive hydroxyl radical imaging. Anal Chem 2019, 91:15757–15762, 10.1021/acs.analchem.9b04002. [PubMed: 31724390]

66. Yang Y, Wang S, Lu L, Zhang Q, Yu P, Fan Y, Zhang F: NIR-II chemiluminescence molecular sensor for in vivo high-contrast inflammation imaging. Angew Chem Int Ed 2020, 59: 18380–18385, 10.1002/ange.202007649.

67. Li D, Wang S, Lei Z, Sun C, El-Toni AM, Alhoshan MS, Fan Y, Zhang F: Peroxynitrite activatable NIR-II fluorescent molecular probe for drug-induced hepatotoxicity monitoring. Anal Chem 2019, 91:4771–4779, 10.1021/acs.analchem.9b00317. [PubMed: 30808169]

68. Zhao M, Li B, Wu Y, He H, Zhu X, Zhang H, Dou C, Feng L, Fan Y, Zhang F: A tumor-microenvironment-responsive lanthanide-cyanine FRET sensor for NIR-II luminescence-lifetime in situ imaging of hepatocellular carcinoma. Adv Mater 2020, 32:2001172, 10.1002/adma.202001172.

69. Wang R, Chen J, Gao J, Chen J-A, Xu G, Zhu T, Gu X, Gao Z, Zhu W-H, Zhao C: A molecular design strategy toward enzyme-activated probes with near-infrared I and II fluorescence for targeted cancer imaging. Chem Sci 2019, 10: 7222–7227, 10.1039/c9sc02093d. [PubMed: 31588290]

70*. Chen J, Pan H, Wang Z, Gao J, Tan J, Ouyang Z, Guo W, Gu X: Imaging of ovarian cancers using enzyme activatable probes with second near-infrared window emission. Chem Commun 2020, 56:2731–2734, 10.1039/c9cc09158k.The authors present BOD-M-βGal, a β-galactosidase-responsive fluorogenic probe based off of previous enzyme-responsive BODIPY probes. Direct comparisons between NIR and SWIR detection are made by employing NIR probe BOD-K-βGal and BOD-M-βGal for xenograft ovarian cancer imaging.

71. Dou K, Huang W, Xiang Y, Li S, Liu Z: Design of activatable NIR-II molecular probe for in vivo elucidation of disease-related viscosity variations. Anal Chem 2020, 92:4177–4181, 10.1021/acs.analchem.0c00634. [PubMed: 32126756]

72. Bonis-O'Donnell JTD, Page RH, Beyene AG, Tindall EG, McFarlane IR, Landry MP: Dual near-infrared two-photon microscopy for deep-tissue dopamine nanosensor imaging. Adv Funct Mater 2017, 39:1702112, 10.1002/adfm.201702112.

73. Liu D, He Z, Zhao Y, Yang Y, Shi W, Li X, Ma H: Xanthene-based NIR-II dyes for *in vivo* dynamic imaging of blood circulation. J Am Chem Soc 2021, 143:17136–17143, 10.1021/jacs.1c07711. [PubMed: 34632770]

74. Yao D, Wang Y, Zou R, Bian K, Liu P, Shen S, Yang W, Zhang B, Wang D: Molecular engineered squaraine nanoprobe for NIR-II/photoacoustic imaging and photothermal therapy of meta-static breast cancer. ACS Appl Mater Interfaces 2020, 12: 4276–4284, 10.1021/acsami.9b20147. [PubMed: 31896256]

75. Zhang W, Deng W, Zhang H, Sun X, Huang T, Wang W, Sun P, Fan Q, Huang W: Bioorthogonal-targeted 1064 nm excitation theranostic nanoplatform for precise NIR-IIa fluorescence imaging guided efficient NIR-II photothermal therapy. Bio-materials 2020, 243:119934, 10.1016/j.biomaterials.2020.119934.

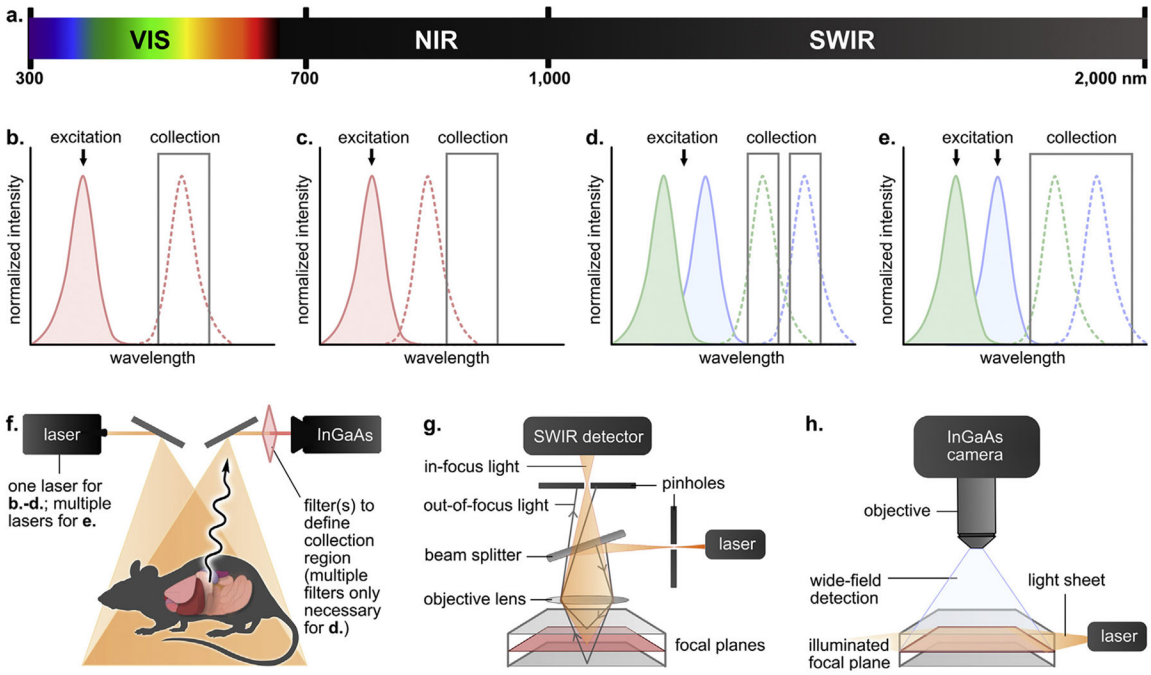

Figure 1.

Established technologies for SWIR bioimaging. **a.** Electromagnetic spectrum with defined visible (VIS), near infrared (NIR) and shortwave infrared (SWIR) regions. Spectral representations of **b.** Traditional single-color imaging, **c.** Fluorescence tail imaging, **d.** Emission-multiplexed imaging, and **e.** Excitation-multiplexed imaging. Absorption and emission traces are indicated by shaded and dotted curves, respectively. **f.** Generalized whole-animal imaging setup. Schematized **g.** confocal and **h.** light-sheet microscopy setups for three-dimensional imaging.

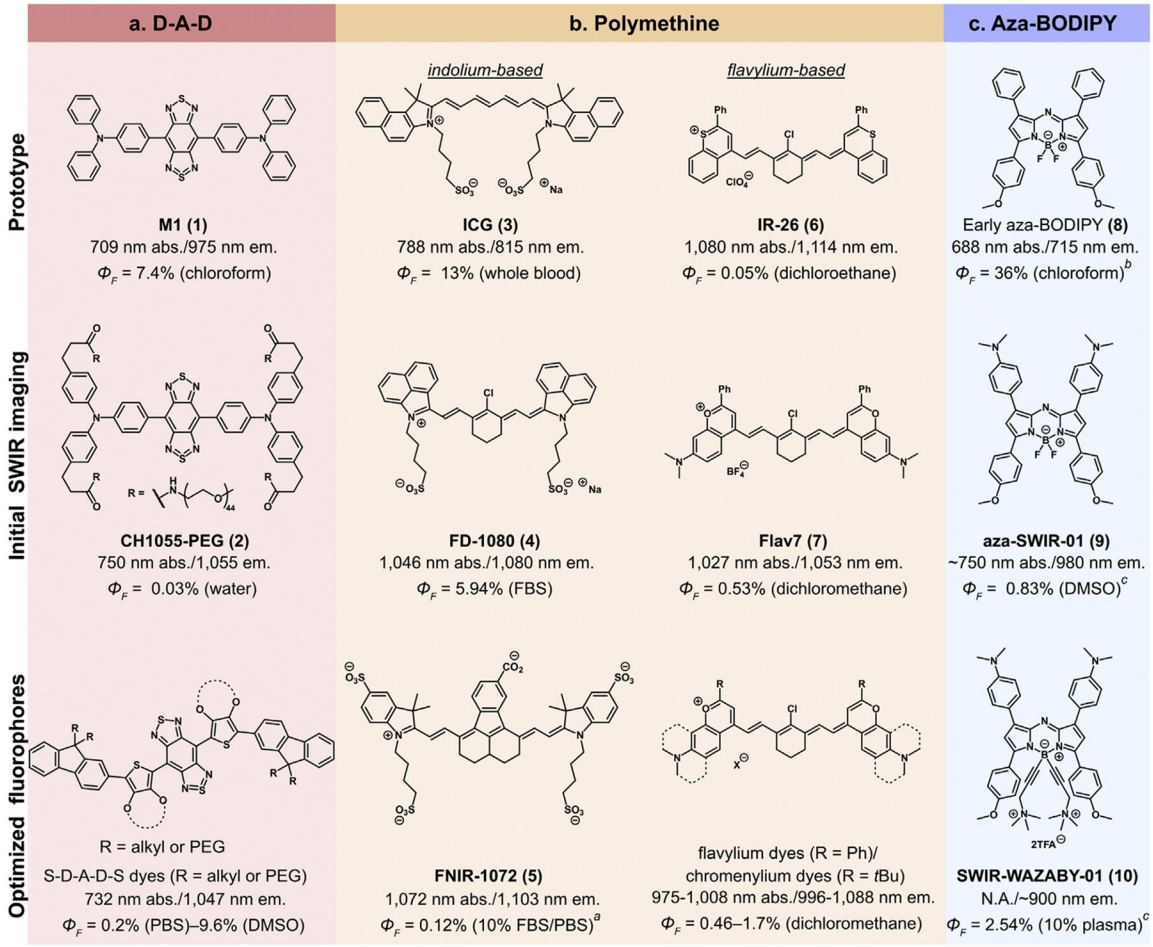

Figure 2.

Tuning of pre-existing **a.** donor-acceptor-donor, **b.** polymethine, and **c.** aza-BODIPY scaffolds into SWIR-emissive dyes for improved imaging *in vivo*. All values were calculated relative to IR-26 (Φ_F = 0.05% in dichloroethane) as a reference unless otherwise noted. [a]IR-26 (Φ_F = 0.11% in dichloroethane) used as a reference. [b]Magnesium tetra-*tert*-butyl phthalocyanine (Φ_F = 84% in chloroform) used as a reference. [c]IR-125 (Φ_F = 23% in DMSO) used as a reference.

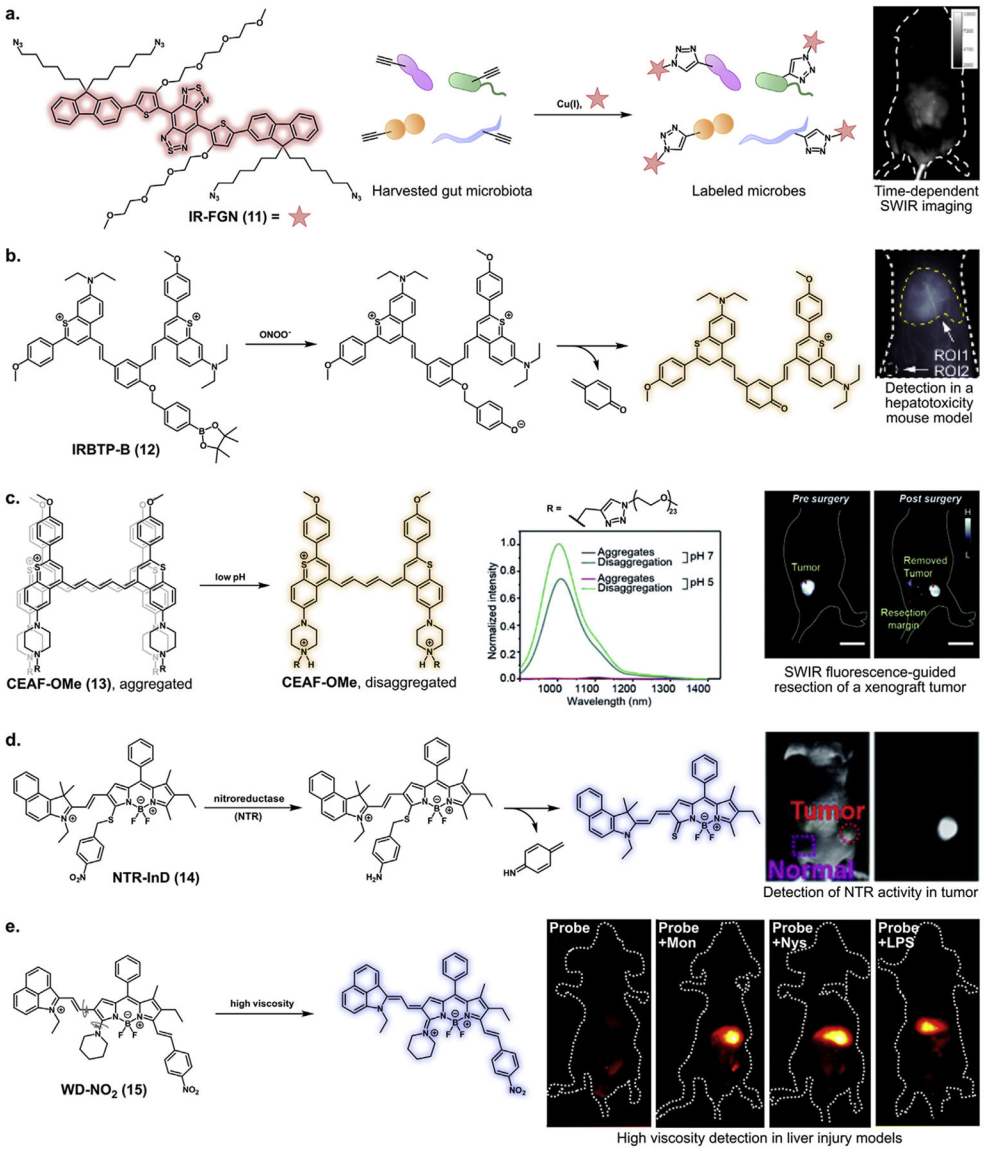

Figure 3.

Targeting and activation mechanisms for select SWIR probes. **a.** Conjugation of **IR-FGN** to metabolically incorporated *D*-propargyl glycine facilitates *in vivo* tracking of gut microbiota. © 2019 Wiley-VCH Verlag GmbH & Co. KGaA, Weinheim. **b. IRBTP-B** fluorescence is activated through boronate ester cleavage by peroxynitrite and spontaneous elimination of p-quinone methide. This probe was used for detection in an acetaminophen-induced livery injury model. Reprinted (adapted) with permission from ref 67. Copyright 2019, American Chemical Society. **c.** Protonation of **CEAF-OMe** in lysosomes disrupts aggregation induced quenching, yielding bright SWIR fluorescence for image-guided surgery. Scale bar represents 2 cm. Reproduced from ref 63 with permission from the Royal Society of Chemistry. **d.** Reduction of the nitro group and spontaneous elimination of a 2,5-cyclohexadiene imine activates nitroreductase-responsive probe **NTR-InD** in a xenograft mouse model. Reproduced from ref 69 with permission from the Royal Society

of Chemistry. **e.** Rigidification of a piperidinyl moiety favors fluorescence of probe **WD-NO_2** in a high viscosity liver models induced by monensin (Mon), nystatin (Nys), and lipopolysaccharide (LPS). Reprinted (adapted) with permission from ref 71. Copyright 2020, American Chemical Society.

Table 1

Characteristics of recently reported D-A-D, polymethine, and BODIPY-based SWIR probes.

Entry	Probe	Mechanism	Target/trigger	$\lambda_{max,abs}/\lambda_{max,em}$ (nm)	Φ_F (%)	Ref.
D-A-D						
1	TTQ-PLL@OVA	Molecular imaging	Dendritic cells	740/1050	1.24[a] (water)	[60]
2	IR-FGN	Molecular imaging	*D*-propargyl glycine	745/1050	1.9[b] (water)	[23,61]
3	NIR-II-CLS	Ratiometric	Peroxynitrite	540/680; 700/985	N.A.	[66]
Polymethine						
4	ICG-C11-Herceptin	Molecular imaging	HER2	1021/1058	1.3[c] (DMSO)	[49]
5	FNIR-1072-Dex	Molecular imaging	Lymphatic system	1072/1103	0.055[d] (10% FBS/PBS)	[50]
6	5H5-PEG_8-$cRGD_{fk}$	Molecular imaging	$\alpha_v\beta_3$ integrin	1069/1125	0.26[e] (acetonitrile)	[52]
7	QT-RGD	Molecular imaging	$\alpha_v\beta_3$ integrin	1042/1068	0.12[e] (DMSO)	[62]
8	CEAF-RGD	Molecular imaging	$\alpha_v\beta_3$ integrin	980/1017	0.20 (dichloromethane)	[63]
9	IRBTP-B	Fluorogenic	Peroxynitrite	785/970	0.10 (methanol)	[67]
10	CEAF-OMe	Fluorogenic	Endocytosis, pH	980/1017	0.20 (dichloromethane)	[63]
11	PN1100	Ratiometric	Peroxynitrite	883[f]/920; 1089/1140	0.66[f]; 0.091 (chloroform)	[54]
12	DSNP@MY-1057	Ratiometric	Peroxynitrite	N.A./1060; 1057/1081	N.A.; 0.71 (DMSO)	[68]
BODIPY						
13	BTC1070	Ratiometric	pH	~600–900/1015; 980/1,065[g]	N.A.; 0.016[g] (PBS)	[51]
14	NTR/NQO/ALP-InD	Fluorogenic	NTR, NQO, ALP	730/900	0.048[h] (DMSO/TRIS-HCl)	[69]
15	BOD-M-βGal	Fluorogenic	β-galactosidase	723/853	N.A.	[70]
16	WD-NO_2	Fluorogenic	Viscosity	818/982	0.3128[c] (glycerol)	[71]

Photophysical values reflect dyes prior to nanoparticle formulation or conjugation with targeting agents unless otherwise stated. Values for fluorogenic probes reflect the emissive state. For ratiometric probes, values for each fluorescent component are listed in order of increasing $\lambda_{max,abs}$. To facilitate probe comparison, all Φ_F values were calculated to be referenced to IR-26 Φ_F = 0.05% in dichloroethane or IR-1061 Φ_F = 0.32% in dichloromethane. All instances where a recalculation was performed due to a different reference in the original report are noted. Otherwise reported values were calculated relative to IR-26 Φ_F = 0.05% in dichloroethane).

[a] IR-1061 used as a reference but no Φ_F or solvent reported for the reference.

[b] HiPco carbon nanotubes used as a reference.

[c] Recalculated with IR-1061 (Φ_F = 0.32% in dichloromethane) as a reference.

[d] Recalculated with IR-26 (Φ_F = 0.05% in dichloroethane) as a reference.

[e] Listed value is for dye–peptide conjugate.

[f] 1% trifluoroacetic acid was added to obtain these values.

[g] Determined from dye loaded into phospholipid micelles. First and second set of values refer to probe below and above pH 4, respectively.

[h] A reference fluorophore was not reported for Φ_F calculations.